Inorganic Chemistry

Article

pubs.acs.org/IC

Compressibility and Structural Stability of Nanocrystalline TiO_2 Anatase Synthesized from Freeze-Dried Precursors

Catalin Popescu,*[,†] Juan Angel Sans,[‡] Daniel Errandonea,[§] Alfredo Segura,[§] Regina Villanueva,[∥] and Fernando Sapiña[∥]

[†]CELLS-ALBA Synchrotron Light Facility, 08290 Cerdanyola, Barcelona, Spain

[‡]Instituto de Diseño para la Fabricación y Producción Automatizada, MALTA Consolider Team, Universitat Politècnica de València, 46022 València, Spain

[§]ICMUV-Departamento de Física Aplicada, MALTA Consolider Team, Universitat de València, 46100 Burjassot, Spain

[∥]Institut de Ciencia dels Materials, Universitat de València, Apartado de Correos 22085, E-46071 València, Spain

ABSTRACT: The high-pressure structural behavior of 30 nm nanoparticles of anatase TiO_2 was studied under hydrostatic and quasi-hydrostatic conditions up to 25 GPa. We found that the structural sequence is not sensitive to the use of different pressure transmitting media. Anatase-type nanoparticles exhibit a phase transition beyond 12 GPa toward a baddeleyite-type structure. Under decompression this phase transition is irreversible, and a metastable columbite-type structure is recovered at ambient conditions. The bulk modulus of anatase-type nanoparticles was determined confirming that nanoparticles of TiO_2 are more compressible than bulk TiO_2. Similar conclusions were obtained after the determination of the bulk modulus of baddeleyite-type nanoparticles. Furthermore, axial compressibilities and the effect of pressure in atomic positions, bond distances, and bond angles are determined. Finally, a possible physical explanation for the destabilization of anatase under pressure is proposed based upon this information.

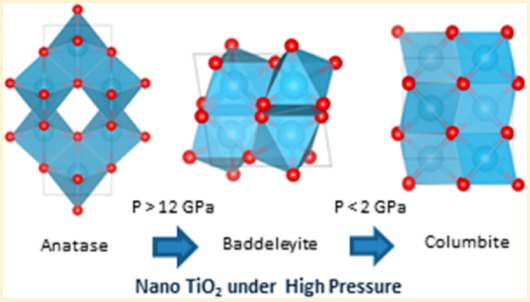

1. INTRODUCTION

High-pressure (HP) investigations of nanomaterials developed in parallel to the growth of nanosciences to better understand the properties of nanomaterials.[1] In particular, pressure-induced structural phase transitions in nanocrystalline TiO_2 (nc-TiO_2) have attracted much attention because of their unique behavior.[2−5] TiO_2 is considered as an excellent model for the study of the nanomechanical properties of ceramic systems. Previous studies indicate that the HP behavior of nc-TiO_2 depends largely upon the particle size.[2−6] In anatase-type nc-TiO_2, pressure-induced amorphization occurs when particle size is less than 10 nm and crystal−crystal transitions take place in coarser particles. However, it has been reported recently that the surface state and defect density in the nanoparticles could strongly modify their HP behavior.[7] The compressibility of anatase-type nc-TiO_2 has been already explored. Previous studies are controversial, showing that the bulk modulus of nc-TiO_2 may either decrease or increase with the particle size.[8] Recently, this subject has been systematically studied, showing that the decrease of particle size produces an increase in compressibility,[8] suggesting an inverse Hall-Petch behavior in anatase-type nc-TiO_2. In addition to particle size, there are other facts that could influence the HP behavior of nc-TiO_2; one is the selection of the pressure-transmitting medium (PTM) used in high-pressure experiments. Depending on the PTM, the pressure gradient and deviatoric stresses inside the pressure chamber are different. This fact may have a strong influence on the physical state of the studied sample.[9−11] In addition, it cannot be ignored the interaction between the nanocrystalline sample and the PTM due to the high surface-to-volume ratio of nanomaterials and the tendency of nanoparticles to aggregate.[12] In the case of anatase-type nc-TiO_2, it has been argued that the use of different PTM in experiments might lead to different results.[12] To contribute to the understanding of the HP behavior of anatase-type nc-TiO_2, we carried out HP X-ray diffraction (XRD) studies on 30 nm size nanoparticles. High-quality data were collected using a synchrotron X-ray source (ALBA). Experiments were carried out using two different PTM: a mixture of 16:3:1 methanol−ethanol−water (MEW), which serves as a quasi-hydrostatic PTM, and helium (He), which is hydrostatic. We have found in both cases crystalline−crystalline phase transitions at similar pressures. We also studied in detail the bulk and polyhedral compressibility of the low- and high-pressure phases of nc-TiO_2. In addition, the behavior of the interatomic distances under pressure was investigated. The obtained results will be compared with previous studies.[2−8,12]

Received: July 12, 2014
Published: October 22, 2014

   dx.doi.org/10.1021/ic501571u | *Inorg. Chem.* 2014, 53, 11598−11603

2. EXPERIMENTAL METHODS

In the present study we used anatase-type nc-TiO_2 powders prepared by thermal decomposition at low temperatures of precursors obtained by freeze-dying of appropriate solutions, as described by Villanueva et al.[13] The anatase structure [space group (SG) $I4_1/amd$, No. 141, Z = 4] was confirmed by XRD in a Bruker AXS-5005 diffractometer using a Cu Kα radiation. According to the Bragg peaks full-width-half-maximum, a particle size of 30(4) nm is estimated from the Scherrer equation.[14] The morphology of the nanoparticles was explored using scanning and transmission electron microscopes (SEM: Hitachi 4100FE, TEM: Jeol JEM 1010). These studies showed that the prepared TiO_2 sample was constituted by aggregates of pseudospherical particles with sizes comprised between 25−35 nm, which agrees with the particle size determined from XRD.

To remove moisture from the sample, it was dried before the experiments for 24 h at 60 °C. Two series of HP XRD experiments were performed: one up to 24.8 GPa using MEW as PTM, and another up to 19.8 GPa using He as PTM. We completed the pressure cycle, following the evolution of the structure under compression and also under decompression. Angle-dispersive XRD experiments were carried out using diamond−anvil cells (DAC) with diamond culets of 300 μm. The pressure chamber was a 100 μm hole drilled on a 40 μm preindented inconel gasket. XRD experiments were performed at the MSPD beamline at ALBA synchrotron facility.[15] The beamline is equipped with Kirkpatrick−Baez mirrors, to focus the X-ray beam to 20 μm × 20 μm, and a Rayonix CCD detector. We used a wavelength of 0.4246 Å and a sample−detector distance of 280 mm. Diffraction images were integrated with FIT2D software.[16] Pressure was determined using Cu as pressure scale[17] in the MEW experiment and with the ruby scale[18] in the He experiment. In both cases, pressure was measured with an accuracy of 0.05 GPa. Structural analysis was performed with GSAS.[19]

3. RESULTS AND DISCUSSION

XRD patterns taken on 30 nm anatase-type nc-TiO_2 at different pressures are shown in Figures 1 and 2. In the He experiment

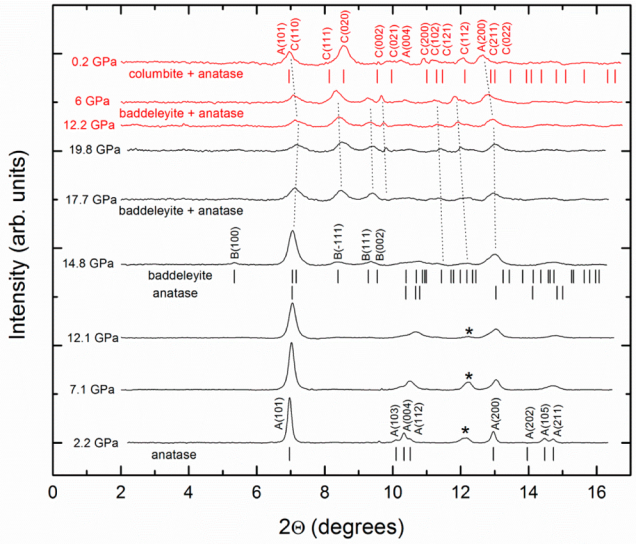

Figure 1. X-ray diffraction patterns measured at selected pressures using He as PTM. In the anatase pattern measured at 2.2 GPa, the Bragg peaks are indexed and labeled. In the pattern measured at 14.8 GPa, the most characteristic peaks of the baddeleyite structure are indicated. The three traces on the top correspond to diffraction patterns measured on decompression. In the top pattern (0.2 GPa), the most intense peaks of anatase and columbite are labeled. Ticks indicate the calculated positions of Bragg peaks for the different structures. The asterisks denote gasket peaks.

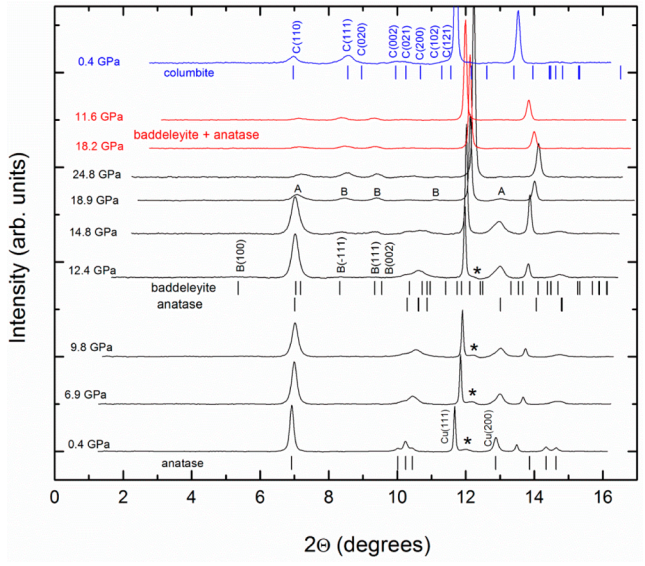

Figure 2. X-ray diffraction patterns measured at selected pressures using MEW as PTM. In the pattern measured at 12.4 GPa the most characteristic peaks of the baddeleyite structure are indicated. The three traces on the top correspond to diffraction patterns measured on decompression. In the top pattern (0.2 GPa), the most intense peaks of columbite are labeled. Ticks indicate the calculated positions of Bragg peaks for different structures. The asterisks denote gasket peaks. The Cu peaks used to determine pressure are identified in the bottom trace.

(Figure 1) there is no substantial broadening in the Bragg peaks up to 12.1 GPa. In addition to eight Bragg peaks belonging to the anatase phase, labeled and indexed in Figure 1, we can observe the appearance of a broad peak coming from the gasket material and identified with an asterisk in the figure. The unit-cell parameters of anatase at ambient conditions are a = 3.786(1) Å and c = 9.516(2) Å. At 14.8 GPa, the Bragg peaks of anatase become broader and they start to lose intensity, as new broad bands start to appear. These bands become more noticeable when the pressure increases. All these new peaks can be assigned to the baddeleyite structure (SG $P2_1/c$, No. 14, Z = 4). Ticks indicating the calculated positions for baddeleyite Bragg peaks are shown in Figure 1. The baddeleyite phase coexists with anatase up to the highest pressure covered by the experiment. At 19.8 GPa baddeleyite predominates and its peaks are broad, indicating a pressure-induced disorder but not amorphization. This result confirms the conclusions extracted by Wang et al.[12] from experiments carried out using less hydrostatic pressure media: in contrast with bulk anatase, anatase-type nc-TiO_2 with 12−50 nm particle size transforms into baddeleyite-type without going through the columbite-type structure (SG $Pbcn$, No. 60, Z = 4). According to our experiments, at 14.8 GPa, the lattice parameters of baddeleyite are a = 4.566(6) Å, b = 5.178(9) Å, c = 4.736(7) Å, and β = 98.7(1)°. Upon decompression, we observed the coexistence of baddeleyite and anatase to 6 GPa. After full decompression, at 0.2 GPa we found a XRD pattern that cannot be assigned to baddeleyite and/or anatase. The new peaks that appear upon decompression can be assigned to the columbite structure which is recovered upon decompression. A minor contribution of the anatase phase is also present. At 0.2 GPa the lattice parameters of columbite are a = 4.497(4) Å, b = 5.565(6) Å, and c = 4.939(5) Å.

dx.doi.org/10.1021/ic501571u | Inorg. Chem. 2014, 53, 11598−11603

On the other hand, the experiment performed with MEW as PTM showed very similar results (see Figure 2), with pure anatase being detected up to 9.8 GPa and baddeleyite and anatase coexisting from 12.4 GPa up to 24.8 GPa. In this case at 12.4 GPa the lattice parameters of baddeleyite are a = 4.599(9) Å, b = 5.097(8) Å, c = 4.763(7) Å, and β = 99.5(3)°. Upon decompression, XRD patterns show the coexistence of the columbite structure with the baddeleyite phase below 3.1 GPa in the decompression process. In this second run, a pure columbite structure was found when the pressure was released. At 0.4 GPa the lattice parameters of columbite are a = 4.493(8) Å, b = 5.562(7) Å, and c = 4.911(6) Å. These values are comparable with previous reported values[20] and their bulk counterparts.[21] It must be stressed that the transition from anatase to baddeleyite implies a volume decrease of about −16%. At ambient conditions the volume decrease from anatase to columbite is about −10%; that is, the density of columbite is between the density of anatase and baddeleyite.

Before discussing in detail the pressure effects on anatase TiO_2, we would like to compare our results with a previous study[12] done for similarly sized nanoparticles. In that study, Wang et al.[12] showed that comparable results are obtained when particles of nanoanatase are squeezed independently of the PTM used in the experiments. They used 4:1 methanol−ethanol and silicone oil in their experiments. Under these experimental conditions deviatoric stresses are known to be larger than in our experiments. In spite of it, here, using MEW and He as PTM, we reached the same conclusions than Wang et al.[12] A conclusion that can be obtained from these results is that the influence of deviatoric stresses on the HP structural behavior of nc-TiO_2 anatase can be neglected in the pressure range here studied. This conclusion contradicts that the interface energy between the pressure-transmitting medium and nanoparticles undoubtedly modifies the phase stability of anatase TiO_2 during high-pressure experiments.[12]

To obtain quantitative information on the structural properties of anatase, Rietveld refinements were performed with both set of data in the pressure range where only pure anatase is observed (up to 12.1 or 9.8 GPa, depending on the experiment). Representative profile fittings are shown in Figure 3, where the top panel corresponds to the He experiment and the bottom panel to the MEW experiment. The residuals of the Rietveld refinements are also shown in Figure 3. It can be seen that the agreement between the theoretical and experimental diffraction patterns is quite good. The residuals from all refinement are R_{wp} = 2.4−3.1%, R_p = 1.8−2.5%, while the goodness of the fit is χ^2 = 0.5−1. The background is subtracted in the figure but considered in the fit. The refinements quality is comparable with state-of-the art HP diamond-anvil cell XRD experiments.[22,23] Similar quality refinements were obtained at all pressure for pure anatase. From the Rietveld refinements we obtained unit-cell parameters and atomic coordinates at different pressures for anatase-type nc-TiO_2. It must be stressed that, at ambient pressure, the obtained results agree with the literature:[8,24] a = 3.786(1) Å and c = 9.516(2) Å. For the atomic position of the oxygen atoms we obtained z = 0.1591(2), being this the only atomic coordinate not fixed by symmetry.

In Figure 4 we show the equation of state (EOS) of anatase nanocrystals obtained from both experiments. In the figure it can be clearly seen than our nanoparticles are more compressible than their bulk counterpart. Figure 4 also shows the evolution of the lattice parameters of anatase nanocrystals

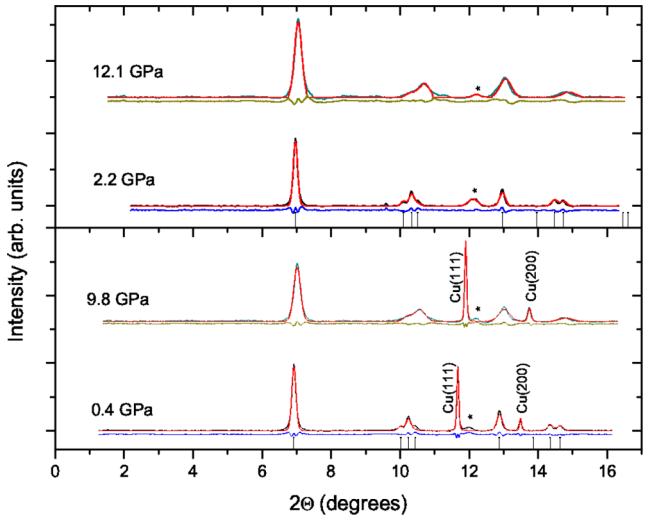

Figure 3. X-ray diffraction patterns and Rietveld refinements of selected patterns of anatase TiO_2. The residuals of the refinements are also shown. The top panel corresponds to the He experiment and the bottom panel to the MEW experiment. Ticks indicate the calculated positions of Bragg peaks for different structures. The asterisks denote gasket peaks. Cu peaks in the MEW experiment are identified.

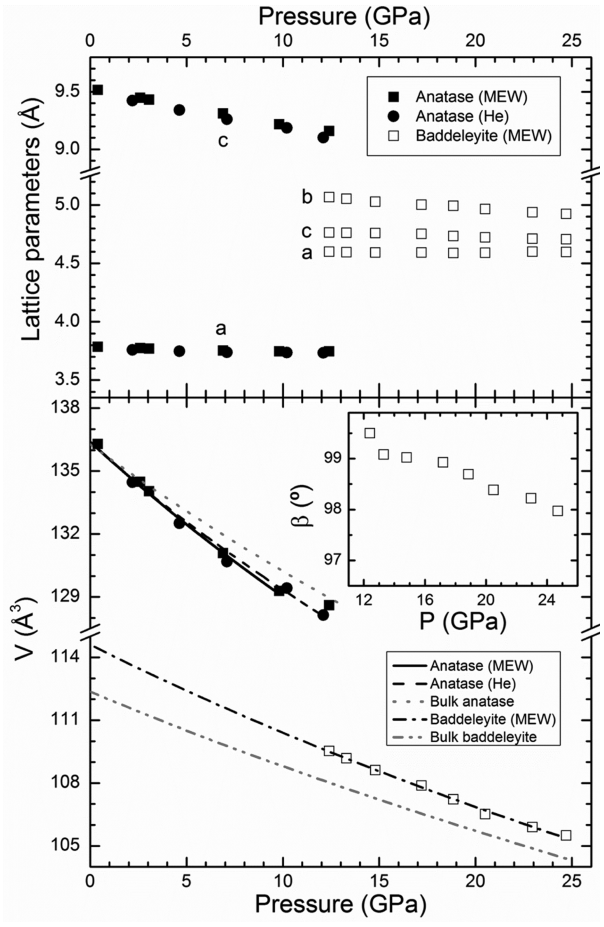

Figure 4. Pressure dependence of the unit-cell volume and lattice parameters obtained for anatase and baddeleyite TiO_2 as determined from present experiments. Symbols: experiments. Lines: EOS fit. Error bars are smaller than symbol sizes. (inset) The evolution of β angle of the baddeleyite phase with pressure. The EOS of bulk anatase and baddeleyite TiO_2 taken from refs 8 and 21 are shown for comparison.

dx.doi.org/10.1021/ic501571u | Inorg. Chem. 2014, 53, 11598−11603

under pressure. The compression of our 30 nm nanoanatase is anisotropic, being the *c*-axis the most compressible one, in accordance with Al-Khatatbeh et al.,[8] who worked with 20 and 40 nm nanoanatase. From our experiments we determined the following axial compressibilities at zero pressure $k_c = (-1/c)(\partial c/dP) = 3.2 \times 10^{-3}$ GPa^{-1} and $k_a = (-1/a)(\partial a/dP) = 1.4 \times 10^{-3}$ GPa^{-1}. Then, nanoanatase is 60% more compressible along the *c*-axis than along the *a*-axis. A similar phenomenon is observed in the thermal expansion of anatase.[24] To determine the bulk modulus (B_0) of nc-TiO_2 anatase, we fit the experimental pressure−volume data with a second-order Birch−Murnaghan (BM) EOS;[25] that is, the pressure derivative of the bulk modulus was fixed to $B_0' = 4$. This assumption was made to facilitate comparison with previous studies,[8] which used a second order BM EOS to describe the pressure dependence of the volume. In these fits, the ambient pressure volume (V_0) was fixed to the value determined in our ambient pressure experiments (V_0 = 136.4 Å^3). We obtained B_0 = 173(4) and 165(4) GPa in the experiments performed under He and MEW, respectively. The EOS fits are shown in Figure 4 with lines. The two values obtained for B_0 agree with the bulk modulus determined for 20 nm particles using MEW as PTM,[8] confirming that the large bulk moduli reported previously for nc-TiO_2 anatase were overestimated (see ref 8 for a detailed discussion). This result also supports that, below a critical particle size, B_0 decreases and remains unchanged at least down to 6 nm size, as concluded by Khatatbeh et al.[8] For 40 nm particles, these authors determined B_0 = 198(10) GPa, which agrees with the bulk modulus of microcrystalline anatase.[8] Thus, it can be established that critical particle size can be constrained between 30 and 40 nm. A possible reason for this observation has been presented by Al-Khatatbeh et al.[8] They suggested that the presence of an extensive average strain when decreasing the particle size (associated with the effective volume increase) is the cause of the unexpected reduction of the bulk modulus. This hypothesis is consistent with our and previous findings. However, a deep exploration of it is beyond the scope of the present work.

Let us comment now on the previous overestimation of B_0 (200 GPa < B_0 < 250 GPa)[2,8] in nc-TiO_2. The main difference between those studies and the experiments reported by Al-Khatatbeh et al.[8] and our experiments is the influence of deviatoric stresses. Previous experiments were carried out under highly nonhydrostatic conditions. In our study, the data used to determine the EOS were collected under conditions where MEW and He behave quasi-hydrostatically.[26] The same condition were fulfilled by the experiments of Khatatbeh et al.[8] Then clearly, nonhydrostaticity can have a large influence of the compressional behavior of nc-TiO_2.

From our experiments measured beyond 12 GPa, we also determined the pressure evolution for the unit-cell parameters (and volume) of the baddeleyite phase. In this case a multiphase LeBail analysis was carried out. This is the first time that such information is reported. Our results are shown in Figure 4. To facilitate comparison with the anatase phase, the variation of the volume with pressure has been fitted to a second order BM EOS.[24] In this case, since the ambient pressure volume (V_0) of baddeleyite is unknown, B_0 and V_0 were assumed free fitting parameters in the EOS. We obtained that V_0 = 114.6 Å^3 and B_0 = 247(9) GPa. Two conclusions can be extracted from this result. First the baddeleyite phase of nc-TiO_2 is much more uncompressible than the anatase phase. This trend, already observed in the bulk counterpart,[21] can be explained in terms of the density increase associated with the phase transition. Second, as it happens in anatase nanoparticles, in the baddeleyite structure our nanoparticles are more compressible than bulk baddeleyite-type TiO_2 (B_0 = 290−303 GPa).[12,21] This can be clearly seen in Figure 4. In the figure it can be also seen than the compression of the baddleyite structure is nonisotropic. In particular, the *b*-axis is the most compressible one and the *a*-axis is nearly uncompressible. The three unit-cell parameters follow a nearly linear dependence with pressure, being the axial compressibilities: $k_a = 1.0 \times 10^{-4}$ GPa^{-1}, $k_b = 2.9 \times 10^{-3}$ GPa^{-1}, and $k_c = 1.1 \times 10^{-3}$ GPa^{-1}. Regarding the monoclinic β angle of baddeleyite, it linearly decreases upon compression from 99.5° at 12.4 GPa to 98° at 24.7 GPa. As a consequence of all these changes, nano-baddeleyite TiO_2 becomes more regular and symmetric upon compression.

To conclude, we comment now on the distortions induced by pressure in anatase-type nc-TiO_2. From the pressure range where the recorded XRD patterns belonged to pure anatase, we determined the pressure evolution of the free atomic coordinate of the oxygen atoms; the only coordinate not determined by symmetry. In both experiments we found that it decreases with pressure from 0.159 at 0.2 GPa to 0.144 at 12.1 GPa. The obtained results are shown in Figure 5. The change of the oxygen free coordinate has consequences on the Ti−O bond distances and the Ti−O−Ti angles. As shown in Figure 6, anatase is formed by chains of TiO_6 octahedral units which share edges. The octahedron is not regular, having two long axial distances and four short equatorial distances (see low-pressure anatase in Figures 6 and 5). Under compression the distortion of the octahedron increases and the difference between the two Ti−O distances is enhanced, as shown in Figure 5. This fact is due to the movement of the oxygen atoms, whose influence on octahedral distortion dominates over the fact that the larger compressibility of the *c*-axis tends to make more regular the octahedron. In addition to determine the influence of pressure on bond distances, it is also interesting to analyze the influence of pressure on the Ti−O−Ti angles. The results obtained for them are also given in Figure 5. There are two angles, one close to 100° and another close to 160° as shown in Figure 6. The first angle gradually decreases under compression approaching 90°. On the other hand, the largest angle becomes larger, reaching a value of 170°. Both facts make the structure more planar, as shown in Figure 6 (see HP anatase), becoming the anatase structure more similar to the rutile structure (Ti and O stay in the same plane with angles of 90° and 180° when they form the rutile structure). This makes the anatase structure unstable, due to the increase of the repulsion between O atoms.[21] We considered that this could be the effect that triggers the transition to baddeleyite TiO_2. Moreover, the transition toward the baddeleyite structure would be energetically more favorable at HP because this structure is more compact than anatase and rutile. The baddeleyite phase is formed by edge-sharing octahedra (as anatase phase) and the rutile phase has a central octahedron that only shares the vertices with the rest of octahedra. This transition also gives rise to an increase of the effective coordination number (5.9 for anatase and 6.2 for baddeleyite), which is a classical effect of the increase of pressure.

4. CONCLUSIONS

We report an experimental study of the compressibility and structural stability of anatase-type nc-TiO_2 with particle size 30

dx.doi.org/10.1021/ic501571u | *Inorg. Chem.* 2014, 53, 11598−11603

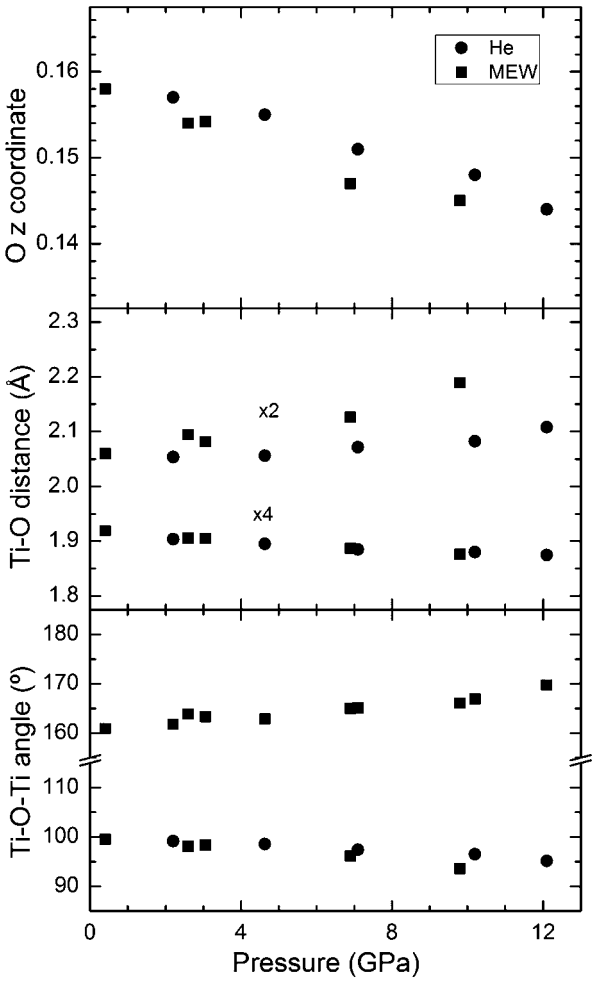

Figure 5. Pressure dependence of z coordinate of the O atom (upper), Ti−O distances (middle), and Ti−O−Ti angles (lower) in anatase TiO_2. Error bars are smaller than symbol sizes. The multiplicity of Ti−O distances is indicated.

nm by high resolution synchrotron powder XRD, using MEW and He as pressure-transmitting media. We found that anatase transforms into the baddeleyite structure beyond 12 GPa, coexisting both phases to the highest pressure covered by the experiments. On pressure release, the observed phase transition is not reversible: TiO_2 transforms into a columbite-type structure, which remains as a metastable phase at ambient conditions. The compressibility of the anatase and baddeleyite phases was determined. For both phases we found that nanoparticles are more compressible than the bulk materials. This result confirms previous findings for anatase nc-TiO_2. The axial compressibility was also determined. In anatase, the c-axis is 60% more compressible than the a-axis. On the other hand, baddeleyite is highly compressible along the b-axis and ultrauncompressible along the a-axis. Finally, the effect of pressure on atomic positions, bond distances, and bond angles causes an increase of the distortion in the TiO_6 octahedra, which leads the anatase to become more planar as pressure increases, resembling the rutile structure. This makes anatase phase unstable and could trigger the observed anatase-baddeleyite transition.

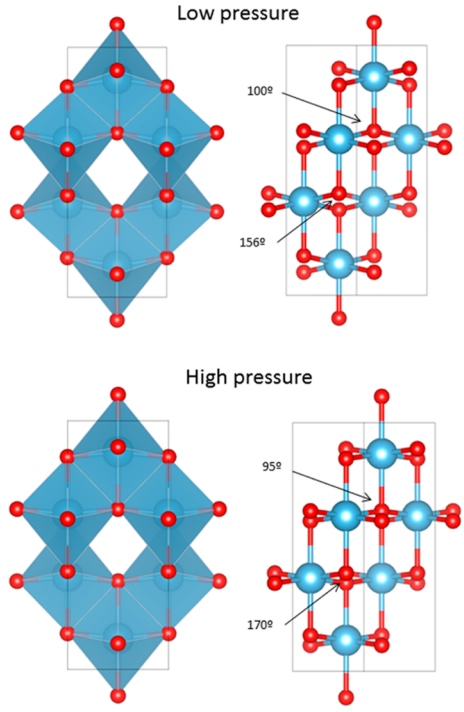

Figure 6. Schematic view of nanocrystalline anatase TiO_2 at ambient pressure (upper) and near 12 GPa (lower). Ti−O−Ti angles are indicated.

AUTHOR INFORMATION

Corresponding Author

*E-mail: cpopescu@cells.es.

Author Contributions

The manuscript was written through contributions of all authors. All authors have given approval to the final version of the manuscript.

Notes

The authors declare no competing financial interest.

ACKNOWLEDGMENTS

Research supported by the Spanish Government MINECO under Grant Nos. MAT2010-21270-C04-01, MAT2012-38364-C03-02, and MAT2013-46649-C04-01 and by Generalitat Valenciana under Grant No. ACOMP/2014/243. J.A.S. acknowledges the Juan de le Cierva fellowship program for financial support.

REFERENCES

(1) San Miguel, A. *Chem. Soc. Rev.* **2006**, *35*, 876−879.
(2) Pischedda, V.; Hearne, G. R.; Dawe, A. M.; Lowther, J. E. *Phys. Rev. Lett.* **2006**, *96*, 035509.
(3) Flank, A. M.; Lagarde, P.; Itie, J. P.; Polian, A.; Hearne, G. R. *Phys. Rev. B* **2008**, *77*, 224112.
(4) Swamy, V.; Kuznetsov, A.; Dubrovinsky, L. S.; McMillan, P. F.; Prakapenka, V. B.; Shen, G.; Muddle, B. C. *Phys. Rev. Lett.* **2006**, *96*, 135702.
(5) Machon, D.; Daniel, M.; Pischeda, V.; Daniele, S.; Bouvier, P.; LeFloch, S. *Phys. Rev. B* **2010**, *82*, 140102(R).
(6) Li, Q.; Chen, B.; Yang, X.; Liu, R.; Liu, B.; Liu, J.; Chen, Z.; Zu, B.; Cui, T.; Liu, B. *J. Phys. Chem. C* **2013**, *117*, 8516−8521.
(7) Piot, L.; LeFloch, S.; Cornier, T.; Daniele, S.; Machon, D. *J. Phys. Chem. C* **2013**, *117*, 11133−11140.
(8) Al-Khatatbeh, Y.; Lee, K. K. M.; Kiefer, B. *J. Phys. Chem. C* **2012**, *116*, 21635−21639.

(9) Gomis, O.; Sans, J. A.; Lacomba-Perales, R.; Errandonea, D.; Meng, Y.; Chervin, J. C.; Polian, A. *Phys. Rev. B* **2012**, *86*, 054121.
(10) Santamaria-Perez, D.; Gracia, L.; Garbarino, G.; Beltran, A.; Chulia-Jordan, R.; Gomis, O.; Errandonea, D.; Ferrer-Roca, Ch.; Martinez-Garcia, D.; Segura, A. *Phys. Rev. B* **2011**, *84*, 054102.
(11) Errandonea, D.; Meng, Y.; Somayazulu, M.; Häusermann, D. *Physica B* **2005**, *355*, 116−125.
(12) Wang, Q.; He, D.; Peng, F.; Lei, L.; Xiong, L.; Wang, P.; Liu, J. *High Pressure Res.* **2014**, *34*, 259−265.
(13) Villanueva, R.; Gomez, A.; Vie, D.; Martinez, E.; Beltran, A.; Sapiña, F.; Vila, J. *J. Am. Ceram. Soc.* **2013**, *96*, 1324−1321.
(14) Guiner, A. *X-ray Diffraction in Crystals, Imperfect Crystals, and Amorphous Bodies;* Dunond: Paris, France, 1956.
(15) Fauth, F.; Peral, I.; Popescu, C.; Knapp, M. *Powder Diffr.* **2013**, *28*, S360−S370.
(16) Hammersley, A. P.; Svensson, S. O.; Hanfland, M.; Fitch, A. N.; Hausermann, D. *High Pressure Res.* **1996**, *14*, 235−248.
(17) Mao, H. K.; Xu, J.; Bell, P. M. *J. Geophys. Res.* **1986**, *91*, 4673−4676.
(18) Dewaele, A.; Loubeyre, P.; Mezouar, M. *Phys. Rev. B* **2004**, *90*, 094122.
(19) Larson, A. C.; von Dreele, R. B. *GSAS: General Structure Analysis System;* Los Alamos National Laboratory: Los Alamos, NM, 2000; Report LA-UR 86−748.
(20) Swamy, V.; Dubrovinskaia, N. A.; Dubrovinsky, L. S. *J. Alloys Compd.* **2002**, *340*, 46−48.
(21) Arlt, T.; Bermejo, M.; Blanco, M. A.; Gerward, L.; Jiang, J. Z.; Staun Olsen, J.; Recio, J. M. *Phys. Rev. B* **2000**, *61*, 14414.
(22) Garg, A. B.; Errandonea, D.; Rodríguez-Hernández, P.; López-Moreno, S.; Muñoz, A.; Popescu, C. *J. Phys.: Condens. Matter* **2014**, *26*, 265402.
(23) Errandonea, D.; Gomis, O.; García-Domene, B.; Pellicer-Porres, J.; Katari, V.; Achary, S. N.; Tyagi, A. K.; Popescu, C. *Inorg. Chem.* **2013**, *52*, 12790−12798.
(24) Burdett, J. K.; Hughbanks, T.; Miller, G. J.; Richardson, J. W., Jr.; Smith, J. V. *J. Am. Chem. Soc.* **1987**, *109*, 3639−3646.
(25) Birch, F. *J. Geophys. Res.* **1978**, *83*, 1257−1268.
(26) Klotz, S.; Chervin, J. C.; Munsch, P.; Le Marchand, G. *J. Phys. D: Appl. Phys.* **2009**, *42*, 075413.